International Journal of Thermophysics, Vol. 14, No. 4, 1993

Sound-Velocity Measurements for HFC-134a and HFC-152a with a Spherical Resonator[1]

T. Hozumi,[2] T. Koga,[3] H. Sato,[2] and K. Watanabe[2]

Received January 14, 1993

A spherical acoustic resonator was developed for measuring sound velocities in the gaseous phase and ideal-gas specific heats for new refrigerants. The radius of the spherical resonator, being about 5 cm, was determined by measuring sound velocities in gaseous argon at temperatures from 273 to 348 K and pressures up to 240 kPa. The measurements of 23 sound velocities in gaseous HFC-134a (1,1,1,2-tetrafluoroethane) at temperatures of 273 and 298 K and pressures from 10 to 250 kPa agree well with the measurements of Goodwin and Moldover. In addition, 92 sound velocities in gaseous HFC-152a (1,1-difluoroethane) with an accuracy of $\pm 0.01\%$ were measured at temperatures from 273 to 348 K and pressures up to 250 kPa. The ideal-gas specific heats as well as the second acoustic virial coefficients have been obtained for both these important alternative refrigerants. The second virial coefficients for HFC-152a derived from the present sound velocity measurements agree extremely well with the reported second virial coefficient values obtained with a Burnett apparatus.

KEY WORDS: ideal-gas specific heat; HFC-134a; HFC-152a; second acoustic virial coefficient; second virial coefficient; spherical resonator; sound velocity.

1. INTRODUCTION

The depletion of stratospheric ozone by CFSs is one of the most serious issues among global environmental problems. It has led us to study the thermodynamic properties of alternative refrigerants.

The thermodynamic properties of refrigerants in the gaseous phase are fundamental information to reveal the thermodynamic characteristics of

[1] Paper dedicated to Professor Joseph Kestin.

[2] Department of Mechanical Engineering, Faculty of Science and Technology, Keio University, 3-14-1 Hiyoshi, Kohoku-ku, Yokohama 223, Japan.

[3] Department of Printing Press Designing, Mihara Machinery Works, Mitsubishi Heavy Industries, 5007 Itozaki-cho, Mihara 729-03, Japan.

0195-928X/93/0700-0739$07.00/0

refrigerants to be applied in various energy conversion systems. HFC-134a (1,1,1,2-tetrafluoroethane) and HFC-152a (1,1-difluoroethane), which have zero ozone depleting potential and a boiling-point temperature similar to that of CFC-12 (dichlorodifluoromethane), are promising as alternatives to replace CFC-12, which is being used as a working fluid in conventional refrigeration systems. Concerning the thermodynamic properties of HFC-134a and HFC-152a, many *PVT* properties and some caloric properties have been accumulated; among them there exist data on the critical parameters [1, 2], saturated liquid densities and vapor pressures [1, 2], *PVT* properties and vapor pressures [1, 2], *PVT* properties and virial coefficients [1, 2], and equations of state [3–5] reported by our group up to the present.

In order to calculate some caloric properties such as enthalpy and entropy from the equations of state, information about the ideal-gas specific heat is of essential necessity. Sound-velocity measurements are recognized as one of the best approaches to understand the thermodynamic behavior of very dilute gases.

Taking such a background into consideration, we have measured 23 sound velocities in gaseous HFC-134a at temperatures of 273 and 298 K and pressures from 10 to 250 kPa and 92 sound velocities in gaseous HFC-152a at temperatures from 273 to 348 K and pressures from 10 to 250 kPa by means of a spherical acoustic resonator. Not only the ideal-gas specific heats, but also the second acoustic virial coefficients have been derived from the present sound-velocity measurements. And the correlation of the second virial coefficient was developed for HFC-152a.

2. PRINCIPLE OF MEASUREMENTS

2.1. Principle of Sound-Velocity Measurements

According to the description by Mehl and Moldover [6], the first detailed discussion on the theory of spherical acoustic resonances was given in 1896 by Rayleigh and it was then developed to completion by Moldover et al. [7], who reported the universal gas constant with the highest accuracy in 1988 as $R = 8.314471 \pm 0.000014\ \mathrm{J \cdot mol^{-1} \cdot K^{-1}}$.

As illustrated in Fig. 1, the acoustic resonance frequencies in the sample gas within spherical resonator S were produced by serial waves generated by a microphone M_1 (B & K, Type 4134), while they can be detected by a microphone M_2 (B & K, Type 4136). The temperature T, pressure P, frequency f, amplitude A, and phase difference ϕ of resonance frequencies have to be measured. And the series of resonance frequencies

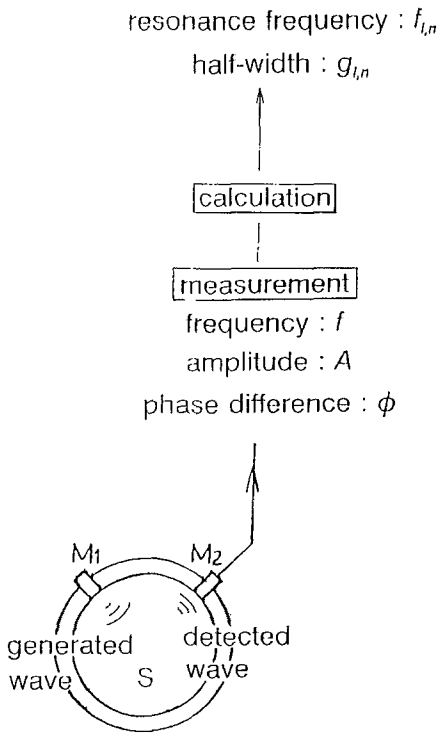

Fig. 1. Principle of sound-velocity measurements by spherical resonator.

$f_{l,n}$ and the half-width $g_{l,n}$ are calculated from the measurements by the following complex expression:[4]

$$u - iv = \frac{ifc}{F_N^2 - f^2} + d + ef \tag{1}$$

where

$$u = A\cos\phi$$

$$v = A\sin\phi$$

$$F_N = f_{l,n} - ig_{l,n}$$

$$c = c_1 - ic_2$$

$$d + ef = (d_1 - id_2) + (e_1 - ie_2)f$$

[4] Nomenclature is given at the end of the paper.

Subscripts l and n denote different frequency modes. The sound velocity W is determined from the values of $f_{l,n}$ and $g_{l,n}$ given by the following complex expression for resonance frequency:

$$f_{l,n} - \mathrm{i}\, g_{l,n} = \frac{WZ_{l,n}}{2\pi a} + \sum_j (\Delta f - \mathrm{i}\, \Delta g)_j \tag{2}$$

where $Z_{l,n}$ is the nth root of the lth-order spherical Bessel function. The values used here are as follows: $Z_{(0,1)} = 4.493$, $Z_{(0,2)} = 7.725$, $Z_{(0,3)} = 10.904$, $Z_{(0,4)} = 14.066$, and $Z_{(0,5)} = 17.221$. The quantity a in the first term of the right-hand side of Eq. (2) denotes the radius of spherical resonator, and the second term is a series of perturbation terms to represent various nonideal conditions. Each frequency mode is expressed by (l, n), where the value of l is zero in the case of radially symmetric modes.

By using a monatomic gas like argon, we are able to determine the radius of spherical resonator because of its known ideal-gas specific heat. Sound velocity W is then expressed by the following virial expansion expression.

$$W^2 = \frac{\gamma^0 RT}{M} + \frac{\gamma^0}{M}\beta_a P + \frac{\gamma^0}{M}\gamma_a P^2 + \cdots \tag{3}$$

β_a is the second acoustic virial coefficient, while γ_a is the third acoustic virial coefficient, respectively. These acoustic virial coefficients give the deviation of the measured sound-velocity value from the ideal sound-velocity value. From Eq. (2) and measurements of $f_{l,n}$ and $g_{l,n}$, we can find the ratio W/a at different pressures for a certain temperature, which is represented as a function of pressure by

$$\left(\frac{W}{a}\right)^2 = \frac{A_0}{a^2} + \frac{A_1}{a^2} P + \frac{A_2}{a^2} P^2 + \cdots \tag{4}$$

where A_0 and A_1, A_2,... are the numerical constants. On the other hand, A_0 fulfills the following thermodynamic relation due to the similarity between Eq. (3) and Eq. (4):

$$A_0 = \frac{\gamma^0 RT}{M} \tag{5}$$

In the case of a monatomic gas, the specific heat ratio γ^0 is 5/3. Then we are able to determine the radius of the spherical resonator by using Eqs. (4) and (5), whereas the sound velocity W is determined simultaneously from the W/a values.

Once a is known, the numerical constants A_0, A_1, and A_2 in Eq. (4) are determined by a least-squares fitting to the measured sound-velocity data. A relation between γ^0 and c_p^0 is given as follows since $c_p^0 = c_v^0 + R$:

$$\gamma^0 = \frac{1}{1 - R/c_p^0} \tag{6}$$

where R denotes the universal gas constant. From Eqs. (5) and (6), we can derive c_p^0, and at the same time, the second acoustic virial coefficient β_a can be determined as

$$\beta_a = \frac{RTA_1}{A_0} \tag{7}$$

2.2. Perturbation Terms

The deviations of the measured frequency from the ideal condition have been carefully discussed by Mehl and Moldover [6]. They corrected such deviations by perturbation terms including a thermal boundary layer term, bulk loss term, shell correction term, imperfect spherical-geometry correction, etc.

The following three major perturbation terms are taken into consideration in the present measurements. The first and dominant perturbation term among them is the effect of thermal boundary layer. The acoustic wave is substantially considered to propagate under an adiabatic process, whereas it becomes isothermal process in the neighborhood of the shell. Such a thermal boundary layer correction is given as follows:

$$(\Delta f - \mathrm{i}\,\Delta g)_{\mathrm{th}} = -(1+\mathrm{i})\frac{\gamma-1}{2a}\sqrt{\frac{D_t f_{l,n}}{\pi}} + \mathrm{i}\frac{(\gamma-1)D_t}{2a^2\pi} + (\gamma-1)\frac{f_{l,n} l_a}{a} \tag{8}$$

where $D_t = \lambda/(\rho c_p)$ is thermal diffusivity.

The first term on the right-hand side of Eq. (8) is the usual thermal boundary layer term, whereas the second term is the correction for the effect of curvature of the wall surface, which is usually small enough in comparison with the first term. We have therefore neglected this second term in the present analysis. The third term in Eq. (8) represents the temperature-jump effect, where the thermal accommodation length l_a is

$$l_a = \frac{\lambda}{P}\sqrt{\frac{\pi MT}{2R}}\frac{(2-h)/h}{c_v/R + 1/2} \tag{9}$$

l_a is inversely proportional to pressure but proportional to the square root of temperature. We calculated the thermal accommodation coefficient h in

Eq. (9) according to the analytical method proposed by Ewing et al. [8], but its magnitude appeared to be insignificant. Therefore the third term on the right-hand side of Eq. (8) was also neglected.

The second perturbation term is the elastic effect of the shell wall. The shell being a rigid body is the ideal condition in the present theory but it behaves as an elastic body in practice. Such a correction for nonideality is represented by

$$\Delta f_{\mathrm{sh}} = \left\{\frac{1+2t^3}{2(t^3-1)}\right\}\left(\frac{\rho W'^2}{\rho_{\mathrm{sh}} W_{\mathrm{sh}}^2}\right)\left\{\frac{f_{l,n}}{1-(f_{l,n}/f_{\mathrm{br}})^2}\right\} \tag{10}$$

where $t = b/a$ with inner radius a and outer radius b of the shell and $W' = 2\pi a f_{l,n}/Z_{l,n}$ is the sound velocity without any perturbation terms. ρ_{sh} denotes the shell density, W_{sh} is the speed of longitudinal waves in the shell material, and f_{br} is the breathing-mode resonance frequency, which is given by

$$f_{\mathrm{br}} = \left(\sqrt{\frac{t^3-1}{2\pi^2(t-1)(1+2t^3)}}\right)\left(\frac{W_{\mathrm{sh}}}{a}\right) \tag{11}$$

The last perturbation term considered is a correction for the acoustic energy dissipation within the viscous fluid:

$$\Delta g_{\mathrm{b}} = \pi\left(\frac{f_{l,n}}{W'}\right)^2 \{(4/3)D_{\mathrm{v}} + (\gamma-1)D_{\mathrm{t}}\} \tag{12}$$

where $D_{\mathrm{v}} = \eta/\rho$ is the kinematic viscosity.

3. EXPERIMENTAL APPARATUS

The experimental arrangement used is illustrated in Fig. 2. The spherical resonator S is placed in the pressure vessel Q, which is immersed in the thermostated bath U. This experimental apparatus consists of three subsystems: signal measuring subsystem, temperature control/measuring subsystem, and pressure measuring subsystem. By the signal measuring system, the frequency, amplitude, and phase difference are measured by frequency synthesizer J and lock-in amplifier K. By the temperature control/measuring subsystem, the temperature is controlled by using a 25-Ω standard platinum resistance thermometer, E_1, with PID controller A and measured by another 25-Ω sheathed standard platinum resistance thermometer, E_2, with a precision AC bridge D_2 (Tinsley, Type 5840D). By the pressure measuring subsystem, the pressure is detected by the quartz

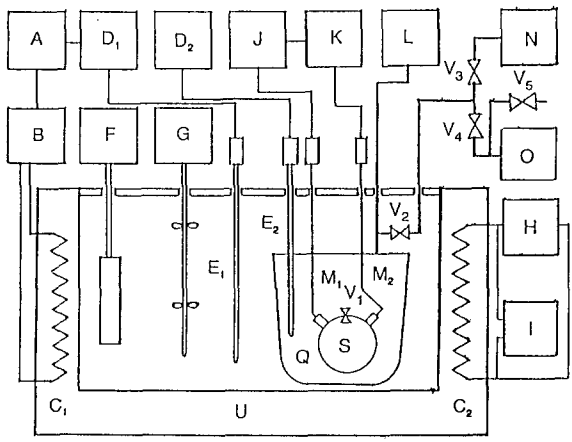

A:PID controller B:Thyristor regulator C_1,C_2:Heaters
D_1,D_2:Thermometer bridges E_1,E_2:Platinum resistance thermometers
F:Cooler G:Stirrer H:Transformer
I:Voltmeter J:Frequency synthesizer
K:Lock-in amplifier L:Pressure gauge M_1,M_2:Transducers
N:Vaccum pump O:Sample bottle Q:Pressure vessel
S:Spherical resonator U:Thermostated bath $V_{1\text{-}5}$: Valve

Fig. 2. Experimental apparatus.

pressure gauge L (Paroscientific, Model 702). The thermostated bath U is filled with water throughout the present measurements.

The present apparatus has been designed for measurements covering temperatures from 243 to 423 K and pressures up to 2 MPa. The pressure vessel Q is made of SUS-304. The upper part is the flange with the connecting pipe for introducing the sample gas into the pressure vessel, the originally designed valve V_1 separates the sample gas from the resonator S, and the sheathed standard platinum resistance thermometer E_2 is mounted through the bore on the flange. The thickness of the flange is 25 mm and the radius of that is 175 mm. The lower part is like a bowl whose thickness is 6.5 mm at the bottom. Figure 3 shows the spherical acoustic resonator, which is made of SUS-304 and consists of two hemispherical parts, (1) and (2). The inner radius of the resonator is about 50 mm, whereas the wall thickness is 20 mm. The inner spherical surface was machined to mirror-finish and we paid full attention to assemble the two halves into perfect spherical alignment.

The upper part (1) is installed with two transducers, a sound generator M_1 and a sound detector M_2, and the valve configuration (3) for

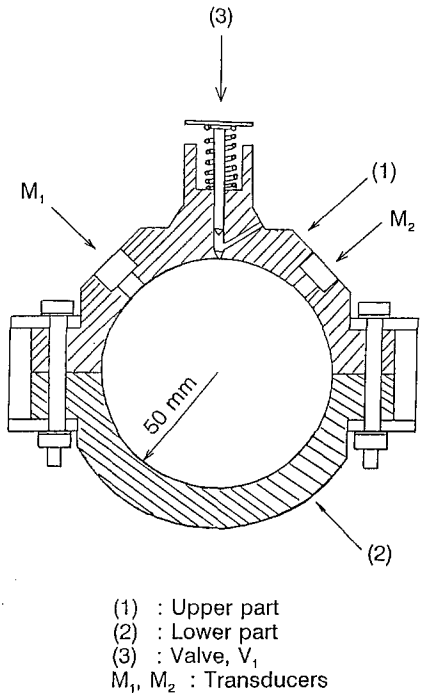

Fig. 3. Spherical resonator.

introducing the sample gas into the resonator. The transducers are set at an angle of 90°. The transducers permit measurements for temperatures below 423 K and frequencies from 0.7 to 20 kHz.

4. EXPERIMENTAL PROCEDURE

After confirming the thermal-equilibrium condition, the temperature and pressure of the sample gas were measured with the sheathed standard platinum resistance thermometer E_2 and pressure gauge L. The frequency, amplitude, and phase difference of the acoustic wave were measured with the lock-in amplifier K and frequency synthesizer J. It takes 10 min to measure all parameters with the aid of a personal computer. When a series of measurements for radially symmetric modes is completed at a prescribed temperature and pressure, we reduce the pressure step by step at the same temperature for succeeding measurements. It takes several days to complete a full series of measurements along a specified isotherm.

5. DETERMINATION OF RESONATOR RADIUS

The inner radius of the spherical resonator at the prescribed temperature is required to deduce the sound velocity. The radius of the resonator is determined accurately from the measurements with monatomic gases. Argon is a monatomic gas whose physical properties are well-known, especially in the dilute gaseous phase. Argon's specific heat ratio should be equal to 5/3. The sound velocity of argon is about $300\ \mathrm{m \cdot s^{-1}}$, which means that five radially symmetric modes are within the range of measurable frequencies. In the case of helium, however, the sound velocity is about $500\ \mathrm{m \cdot s^{-1}}$, which means that only two radially symmetric modes are available. Therefore, we selected argon for the present purpose of determining the resonator radius. In Fig. 4, the measured frequency for gaseous argon at every 2 Hz from 1 to 20 kHz at 273.155 K and 240 kPa is shown as a typical example. The resonance peaks of the radially symmetric modes from (0, 1) to (0, 5) have been observed to be sharper and clearer than those of nonradially symmetric modes.

In this process of assigning modes for respective peaks, we have assumed that the first peak at 2.04 kHz is a non-radially symmetric mode (1, 0) as shown in Fig. 4, since the smallest value $Z_{l,n}$ corresponding to the smallest frequency $f_{l,n}$ should be equivalent to the mode with $Z_{(1,0)}$.

In the ideal condition, the relation between the sound velocity W and the resonance frequency $f^0_{l,n}$ is given by

$$f^0_{l,n} = \frac{WZ_{l,n}}{2\pi a} \tag{13}$$

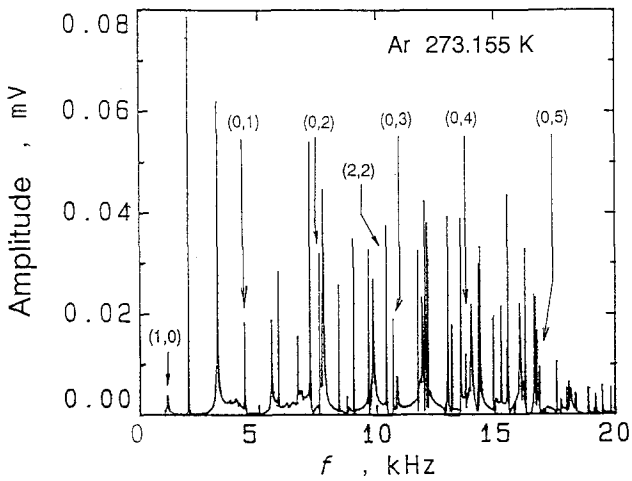

Fig. 4. Overall resonance frequencies in measurements of sound velocities in argon.

If a thermodynamic equilibrium condition is established, the sound velocity W would be a constant at any mode:

$$\frac{f^0_{l,n}}{Z_{l,n}} = \text{const.} \tag{14}$$

The perturbation terms in Eq. (2) which affect the sound velocity to within $\pm 0.01\,\%$ are disregarded in the present study. Hence, we obtain

$$\frac{f^0_{l,n}}{Z_{l,n}} \approx \frac{f_{l,n}}{Z_{l,n}} \tag{15}$$

In order to confirm that the first peak observed at 2.04 kHz is the non-radially symmetric mode (1, 0), we carefully examined the observed peaks in the light of the serial mode numbers thus calculated from Eqs. (14) and (15). One example of the peak observation in frequencies between 10 and 11 kHz for gaseous argon at 273.155 K and 240 kPa is shown in Fig. 5, where the frequency mode (2, 2) is unfortunately non-radially symmetric. Therefore, we could determine the frequencies for the radially symmetric modes from (0, 1) to (0, 5).

The sound velocities in gaseous argon were measured at temperatures from 273 to 348 K (ITS-90) and pressures from 5 to 240 kPa. The data were correlated along each isotherm by a simple linear function of pressure,

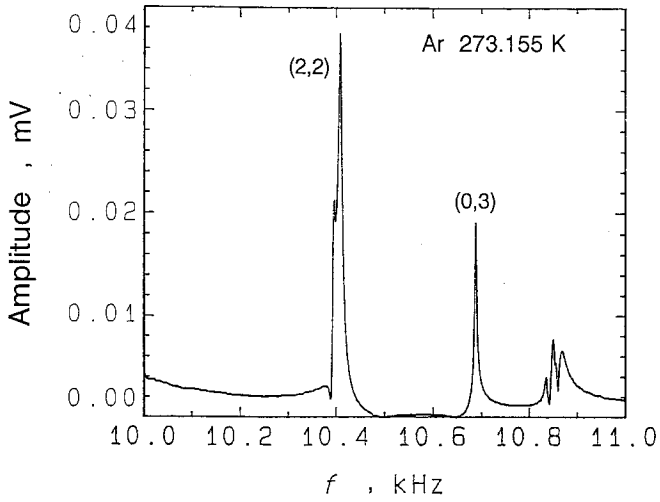

Fig. 5. Typical example of detected resonance frequencies near the mode (0, 3) in measurements of sound velocities in argon.

since argon is a typical ideal gas. The thermophysical properties used to evaluate the perturbation terms for argon are given below:

Second virial coefficient [7]:

$$B = 34.25 - 1.170 \times 10^4 T^{-1} - 9.56 \times 10^5 T^{-2} \tag{16}$$

where B is in $\mathrm{cm^3 \cdot mol^{-1}}$ and T is in K.

Thermal conductivity [7]:

$$\lambda = 16.382 + 0.052(T - 273.16) + 2.16\rho \tag{17}$$

where λ is in $\mathrm{mW \cdot m^{-1} \cdot K^{-1}}$, ρ is in $\mathrm{kg \cdot m^{-3}}$, and T is in K.

Dynamic viscosity [7]:

$$\eta = 20.973 + 0.064(T - 273.16) + 0.01111\rho \tag{18}$$

where η is in $\mu\mathrm{Pa \cdot s}$, ρ is in $\mathrm{kg \cdot m^{-3}}$, and T is in K.

Figure 6 shows the deviation of the present measurements for argon at a temperature of 273.155 K from the proposed correlation of the sound velocity, i.e.,

$$W^2 = 94754.9 + 0.283P \tag{19}$$

where W is in $\mathrm{m \cdot s^{-1}}$ and P is in kPa.

The present measurements are represented by this correlation within $\pm 0.01\%$. The dashed line is a correlation reported by Ewing et al. [8]. The present correlation agrees very well with the correlation by Ewing et al., within 50 ppm.

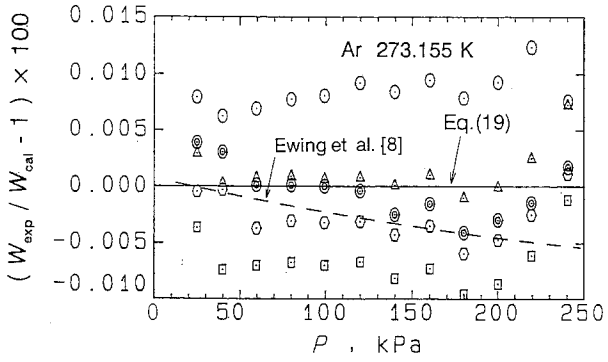

Fig. 6. Deviation from the correlation of sound velocity in argon at 273.155 K. This work: ⊙ (0, 1); △ (0, 2); ⊡ (0, 3); ⊙ (0, 4); ◎ (0, 5).

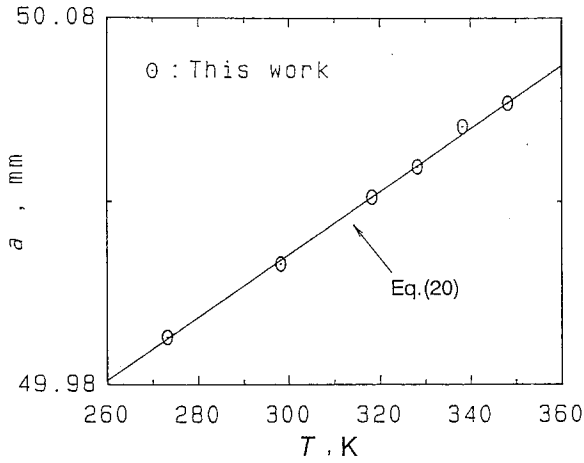

Fig. 7. Deviation from the correlation of the resonator radius.

Based on the sound-velocity measurements for argon along six different isotherms, the inner radius, a, of the resonator was correlated by the function of temperature given below:

$$a = 49.7575 + 8.601 \times 10^{-4} T \tag{20}$$

where a is in mm and T is in K.

Equation (20) reproduces the present measurements within ± 40 ppm and the resonator radius has been determined as shown in Fig. 7. The experimental uncertainties in temperature and pressure measurements are estimated to be ± 11 mK and ± 0.5 kPa, respectively. The purity of argon used was 99.9999 wt%. The uncertainty of the resonator radius is estimated as ± 69 ppm by including the maximum deviation of the measurements from Eq. (20) and systematic error.

6. RESULTS

6.1. Experimental Results for HFC-134a

For HFC-134a, radially symmetric modes from (0, 2) to (0, 5) were determined for each measurement. From those four modes, 23 sound velocities in gaseous HFC-134a were determined at temperatures 273 and 298 K (ITS-90) and pressures from 10 to 250 kPa, as shown in Table I. The

Table I. Sound Velocity for HFC-134a

T_{90} (K)	P (kPa)	W ($m \cdot s^{-1}$)
273.154	189.75	150.961
	170.15	151.686
	150.33	152.408
	130.08	153.134
	109.37	153.865
	90.16	154.536
	68.94	155.264
	50.01	155.905
	29.97	156.576
	10.04	157.235
298.217	251.05	157.474
	230.59	158.049
	210.58	158.603
	190.74	159.146
	170.38	159.699
	150.09	160.243
	130.25	160.773
	110.15	161.303
	90.59	161.815
	70.31	162.341
	50.19	162.856
	30.03	163.373
	10.05	163.888

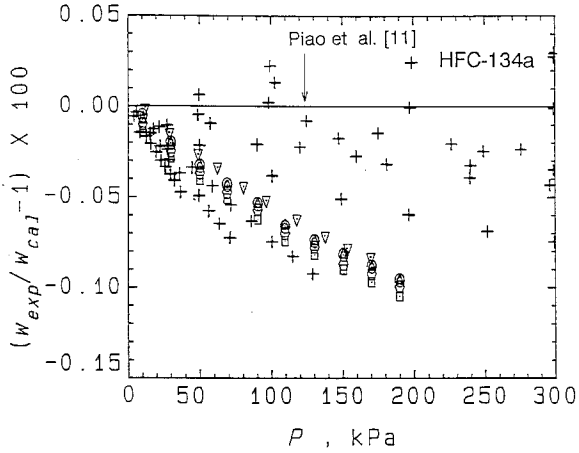

Fig. 8. Deviation from Piao's equation of state [11] for sound velocity in HFC-134a at 273.154 K. This work, 273.154 K: ◬ (0, 2); ⊡ (0, 3); ⊙ (0, 4); ◎ (0, 5). Goodwin and Moldover [9]: ▽, 270 K; +, other temperatures.

measured sound-velocity data were correlated along each isotherm by a guadratic polynomial of the form

$$W^2 = A_0 + A_1 P + A_2 P^2 \tag{21}$$

where A_0, A_1, and A_2 are numerical constants. The thermophysical properties used in the perturbation terms are as follows.

Second virial coefficient [9]:

$$B = 79.95[1 - 1.1006\{\exp(601.6/T) - 1\}] \tag{22}$$

where B is in $\mathrm{cm^3 \cdot mol^{-1}}$ and T is in K.

Ideal-gas specific heat [9]:

$$c_p^0/R = 2.2540 + 0.0317T - 16.8 \times 10^{-6} T^2 \tag{23}$$

where T is in K.

Thermal conductivity [9]:

$$\lambda = 29.742 - 0.1796T + 4.265 \times 10^{-4} T^2 \tag{24}$$

where λ is in $\mathrm{mW \cdot m^{-1} \cdot K^{-1}}$ and T is in K.

The viscosity for gaseous HFC-134a is derived from the following modified Eucken equation [10] with the aid of Eq. (24).

$$\lambda M/\eta = 1.77R + 1.32c_p/\gamma \tag{25}$$

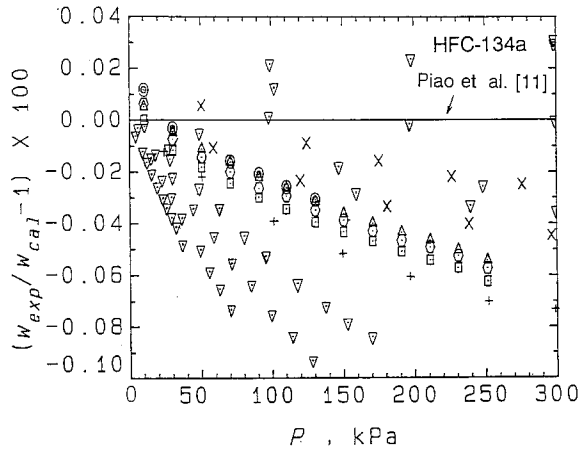

Fig. 9. Deviation from Piao's equation of state [11] for sound velocity in HFC-134a at 298.217 K. This work, 298.217 K: △ (0, 2); ⊡ (0, 3); ◇ (0, 4); ◎ (0, 5). Goodwin and Moldover [9]: +, 290 K; ×, 300 K; ▽, other temperatures.

Table II. Ideal-Gas Specific Heat and Second Acoustic Virial Coefficient for HFC-134a

T_{90} (K)	c_p^0/R	β_a ($cm^3 \cdot mol^{-1}$)
273.154	9.6729	−937.6
298.217	10.2100	−758.2

The present measurements together with the data reported by Goodwin and Moldover [9] are compared with an equation of state developed by Piao et al. [11] in Figs. 8 and 9. Goodwin and Moldover reported sound velocity in gaseous HFC-134a with a claimed accuracy of ±0.01 % for temperatures from 233.16 to 340 K and pressures from 5.6 to 575 kPa. Figure 8 is prepared so as to demonstrate the excellent agreement of the present results along 273.154 K with the data along 270 K by Goodwin and Moldover, while our data along 298.217 K fall between the 290 and the 300 K (2 runs) isotherms reported by them as shown in Fig. 9.

The experimental uncertainties in the temperature and pressure measurements are estimated as ±12 mK and ±0.5 kPa, respectively. The purity of HFC-134a used was 99.98 wt %.

The ideal-gas specific heat c_p^0 and the second acoustic virial coefficient β_a have been determined from the present measurements as given in Table II. The present c_p^0 values together with those reported by Goodwin and Moldover [9] are compared with the correlation developed by Goodwin and Moldover in Fig. 10, while a similar comparison with respect

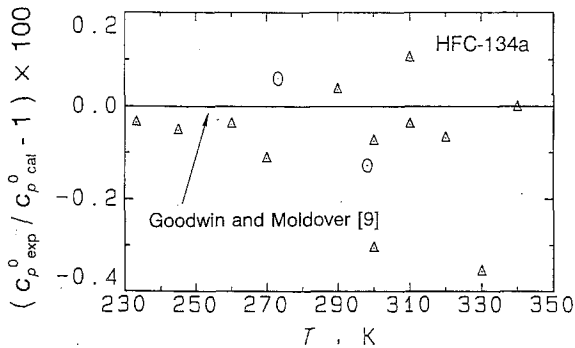

Fig. 10. Deviation from Goodwin's correlation [9] for the ideal-gas specific heat for HFC-134a. (⊙) This work; (△) Goodwin and Moldover [9].

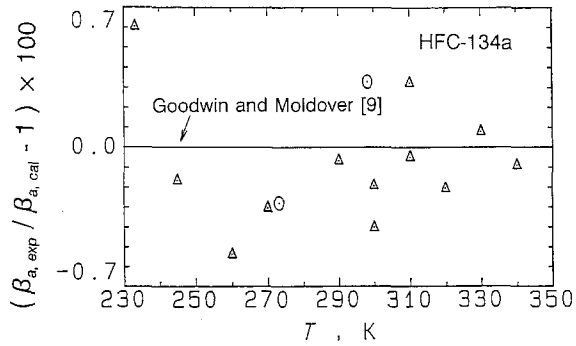

Fig. 11. Deviation from Goodwin's correlation [9] for the second acoustic virial coefficient for HFC-134a. (⊙) This work; (△) Goodwin and Moldover [9].

to β_a is shown in Fig. 11. It becomes clear that the present c_p^0 and β_a values for HFC-134a agree with the respective correlation proposed by Goodwin and Moldover within ± 0.12 and $\pm 0.47\%$, respectively.

6.2. Experimental Results for HFC-152a

Using the correlation for the radius of the resonator given in Eq. (20), we measured 92 sound velocities in gaseous HFC-152a at temperatures from 273 to 348 K (ITS-90) and pressures from 10 to 250 kPa. These

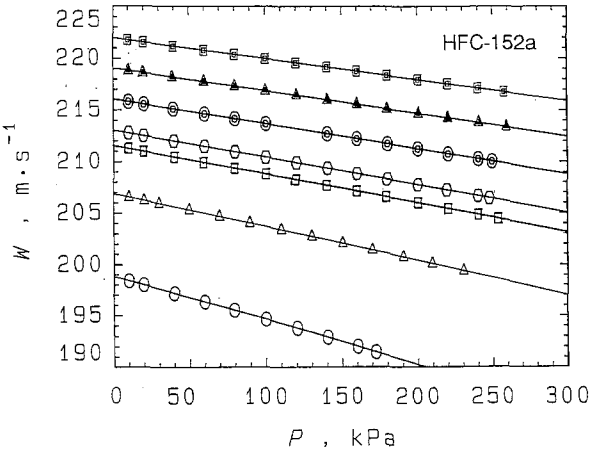

Fig. 12. Present sound-velocity data for HFC-152a. This work: ⊙, 273 K; △, 298 K; ⊡, 313 K; ⊙, 318 K; ◎, 328 K; ⧋, 338 K; ⧈, 348 K.

Table III. Sound Velocity for HFC-152a

T_{90} (K)	P (kPa)	W ($m \cdot s^{-1}$)
273.165	172.17	191.463
	160.13	192.003
	140.19	192.890
	120.26	193.764
	99.91	194.645
	79.48	195.515
	60.07	196.331
	39.88	197.169
	19.48	198.005
	9.83	198.399
298.151	229.98	199.375
	209.15	200.087
	190.04	200.732
	169.95	201.405
	150.17	202.059
	129.80	202.727
	109.98	203.371
	89.47	204.032
	69.66	204.665
	49.76	205.295
	29.88	205.921
	20.00	206.233
	9.97	206.549
313.158	253.43	204.439
	240.20	204.826
	220.31	205.401
	200.22	205.977
	179.39	206.570
	160.05	207.115
	140.07	207.675
	119.70	208.244
	100.10	208.788
	79.82	209.345
	59.26	209.908
	40.10	210.432
	19.89	210.986
	9.83	211.264
318.158	247.66	206.448
	240.03	206.659
	219.41	207.225
	200.13	207.751
	180.01	208.296
	159.91	208.836
	140.19	209.363
	119.99	209.900
	99.98	210.431

Table III. *(Continued)*

T_{90} (K)	P (kPa)	W ($m \cdot s^{-1}$)
	80.03	210.954
	59.99	211.476
	39.86	211.999
	19.85	212.516
	9.96	212.778
328.153	249.22	210.017
	239.99	210.248
	220.01	210.745
	199.89	211.241
	180.05	211.728
	159.83	212.221
	140.12	212.699
	100.12	213.663
	80.03	214.144
	60.06	214.618
	39.52	215.104
	20.03	215.566
	9.95	215.809
338.156	258.96	213.304
	240.49	213.722
	219.92	214.184
	200.28	214.624
	179.86	215.080
	159.91	215.522
	140.25	215.957
	120.13	216.402
	100.03	216.842
	80.00	217.279
	59.90	217.719
	38.91	218.173
	19.87	218.585
	10.03	218.806
348.158	257.55	216.751
	240.04	217.112
	220.03	217.523
	200.39	217.925
	180.07	218.338
	160.02	218.747
	140.14	219.148
	120.06	219.553
	100.10	219.954
	80.10	220.356
	59.99	220.759
	39.81	221.160
	20.13	221.554
	9.96	221.769

results were determined from four radially symmetric modes (0, 2)–(0, 5). The results are presented in Table III and the behavior of the different isothermal sound-velocity measurements are shown in Fig. 12.

The measured sound-velocity data were correlated along each isotherm with Eq. (21). The thermophysical properties used in the perturbation terms are as follows.

Second virial coefficient [12]:

$$\rho_c B = (0.457208 - 1.89826 T_r^{-2}) M \tag{26}$$

where ρ_c is in $kg \cdot m^{-3}$, B is in $dm^3 \cdot mol^{-1}$, M is in $kg \cdot kmol^{-1}$, and $T_r = T/T_c$ is reduced temperature.

Ideal-gas specific heat [13]:

$$c_p^0/R = 3.421564 + 3.937963 T_r + 4.399060 T_r^2 - 1.969414 T_r^3 \tag{27}$$

We used the viscosity values from our own correlation given below, which was developed on the basis of measurements reported by Takahashi et al. [14]

$$\eta = \sum_{j=0}^{2} \left(\sum_{k=0}^{3} m_{j,k} T^k \right) P^j \tag{28}$$

where η is in $\mu Pa \cdot s$ and T is in K.

The numerical constants in Eq. (28) are given in Table IV. The thermal conductivity was derived from the modified Eucken equation, Eq. (25), with the aid of Eq. (28).

Figure 13 shows the deviation of the present measurements at 273.165 K from the proposed correlation, Eq. (21). The measurements at each mode deviate from the correlation systematically but only within ± 60 ppm. Similar agreements were also found for the measurements along other isotherms. The experimental uncertainty in the present sound-velocity measurements is estimated to be not greater than $\pm 0.01\%$, which

Table IV. Viscosity for HFC-152a, Eq. (28)

	k			
j	0	1	2	3
0	4.3631	3.3431×10^{-3}	1.0909×10^{-4}	-1.0236×10^{-7}
1	−14.522	9.4110×10^{-2}	-1.9992×10^{-4}	1.3815×10^{-7}
2	21.909	-1.6952×10^{-1}	4.3862×10^{-4}	-3.7751×10^{-7}

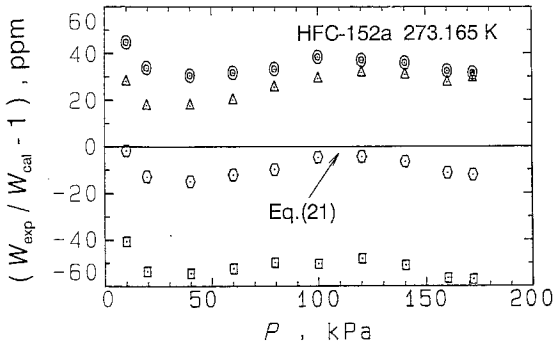

Fig. 13. Deviation from the correlation of sound velocity in HFC-152a at 273.155 K. This work: △ (0, 2); ⊡ (0, 3); ⊙ (0, 4); ◎(0, 5).

includes the scatter of data with four different modes at each temperature. The experimental uncertainties in temperature and pressure measurements are estimated as ±11 mK and ±0.5 kPa, respectively. The purity of HFC-152a used was 99.8 wt%.

The ideal-gas specific heat c_p^0 and the second acoustic virial coefficient β_a have also been determined from the present measurements as given in Table V. The ideal-gas specific heat and the second acoustic virial coefficient are determined by the regression analysis of the present sound-velocity measurements. The standard deviations for c_p^0 and β_a were calculated as ±0.065 and ±0.30%, respectively.

A dimensionless c_p^0 correlation was developed based on the present measurements as

$$c_p^0/R = 3.3390 + 5.47738T_r + 0.972337T_r^2 \tag{29}$$

Table V. Ideal-Gas Specific Heat and Second Acoustic Virial Coefficient for HFC-152a

T_{90} (K)	c_p^0/R	β_a ($cm^3 \cdot mol^{-1}$)
273.165	7.6993	−917.2
298.151	8.1391	−740.9
313.156	8.4074	−662.6
318.158	8.5118	−636.2
328.153	8.7003	−591.6
338.156	8.8805	−553.2
348.158	9.0567	−518.7

Figure 14 shows the deviation of obtained c_p^0 values from the correlation. The dashed line is a correlation reported by McLinden [13]. Our data agree with Eq. (29) within $\pm 0.10\%$ and the maximum difference between our and McLinden's correlations was 0.45% at about 330 K.

On the other hand, β_a was correlated by an expression of the form

$$\beta_a = -5.3662 \times 10^3 + 24.928T - 3.16206 \times 10^{-2}T^2 \tag{30}$$

where β_a is in $cm^3 \cdot mol^{-1}$ and T is in K.

On the basis of the present β_a values, we have also derived the second virial coefficient B so as to compare them with the experimental values of Qian et al. [12], who used the Burnett apparatus for HFC-152a. The thermodynymic relation between β_a and B is given below:

$$\beta_a = 2B + 2(\gamma^0 - 1)T\frac{dB}{dT} + \frac{(\gamma^0 - 1)^2}{\gamma^0}T^2\frac{d^2B}{dT^2} \tag{31}$$

We have simply applied the square-well potential model for B. By calculating Eq. (31) on the basis of the square-well potential model, a trial-and-error approach to find the optimum potential parameters was necessary, and we developed the following expression as the final result:

$$B = 0.69[1 - 67.087\{\exp(735/T) - 1\}] \tag{32}$$

where B is in $cm^3 \cdot mol^{-1}$ and T is in K.

The B values thus calculated from Eq. (32) on the basis of the present β_a values for gaseous HFC-152a are compared with the experimental data and correlation reported by Qian et al. [12] in Fig. 15. They agree well, within $\pm 1\%$ with each other.

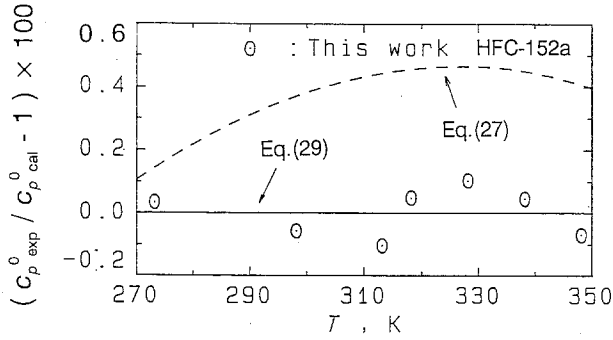

Fig. 14. Deviation from the correlation of the ideal-gas specific heat for HFC-152a.

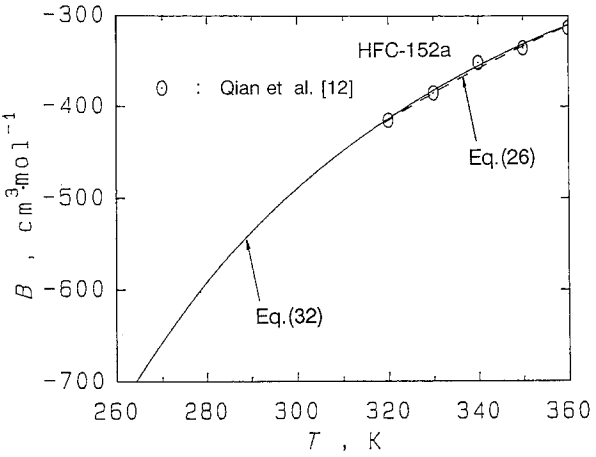

Fig. 15. Comparison with the experimental second virial coefficient values and correlations for HFC-152a.

7. CONCLUSION

Twenty-three sound velocities in gaseous HFC-134a were measured for temperatures 273 and 298 K and pressures from 10 to 250 kPa by means of the spherical acoustic resonator. They agree with the data obtained by Goodwin and Moldover within the respective claimed uncertainties of $\pm 0.02\%$. Ninety-two sound velocities in gaseous HFC-152a were measured at temperatures from 273 to 348 K and pressures from 10 to 250 kPa. The experimental uncertainty in the sound-velocity measurements for HFC-152a was estimated to be not greater than $\pm 0.01\%$.

The ideal-gas specific heat and the second acoustic virial coefficient were deduced from the present measurements with standard deviations of ± 0.065 and $\pm 0.30\%$, respectively. Then the second virial coefficients for gaseous HFC-152a were derived from the present second acoustic virial coefficients with the aid of the square-well potential model. The second virial coefficients thus derived agree with the values experimentally determined by means of the Burnett method in our laboratory within $\pm 1\%$.

ACKNOWLEDGMENT

We thank I. Furutsuka, an undergraduate student, for valuable assistance in measurements and data analysis.

NOMENCLATURE

a	Inner radius of resonator
A	Amplitude
b	Outer radius of resonator
B	Second virial coefficient
c_p	Isobaric specific heat
c_v	Isochoric specific heat
D_t	Thermal diffusivity
D_v	Kinematic viscosity
f	Frequency
f_{br}	Breathing-mode resonance frequency
$f_{l,n}$	Resonance frequency
$g_{l,n}$	Half-width
h	Thermal accommodation length
i	$(-1)^{1/2}$
l_a	Thermal accommodation coefficient
M	Molar mass
P	Pressure
R	Universal gas constant, 8.314471 $J \cdot mol^{-1} \cdot K^{-1}$
T	Temperature
T_c	Critical temperature for HFC-152a, 386.44 K
T_r	Reduced temperature, T/T_c
T_{90}	Temperature (ITS-90)
W	Sound velocity
W'	Measured sound velocity without any perturbation correction
W_{sh}	Speed of longitudinal waves in shell material
$Z_{l,n}$	nth root of lth-order spherical Bessel function

Greek

β_a	Second acoustic virial coefficient
γ	Specific heat ratio
γ_a	Third acoustic virial coefficient
Δf	Perturbation correction for resonance frequency
Δf_{sh}	Perturbation term by the elasticity effect of the shell wall
$(\Delta f - i\,\Delta g)_{th}$	Perturbation term by the effect of the thermal boundary layer
Δg	Perturbation correction for half-width, $\sum (\Delta g)_j = g_{l,n}$
Δg_b	Perturbation term by the correction for the acoustic energy dissipation

η	Viscosity
λ	Thermal conductivity
ρ	Density
ρ_c	Critical density for HFC-152a, 368 $kg \cdot m^{-3}$
ρ_{sh}	Shell density
ϕ	Phase difference

Subscripts

cal	Calculated value
exp	Measured value

Superscript

0	Ideal-gas condition

REFERENCES

1. C.-C. Piao, H. Sato, and K. Watanabe, *ASHRAE Trans.* **96**, Pt. 1:132 (1990).
2. K. Tamatsu, T. Sato, H. Sato, and K. Watanabe, *Proc. Jpn. Symp. Thermophys. Prop.* **12**:189 (1991).
3. K. Tamatsu, T. Sato, H. Sato, and K. Watanabe, *Proc. Jpn. Symp. Thermophys. Prop.* **13**:319 (1992).
4. C.-C. Piao, H. Sato, and K. Watanabe, *Trans. JSME* **57**:192 (1991) (in Japanese).
5. C.-C. Piao, H. Sato, and K. Watanabe, *ASHRAE Trans.* **97**, Pt. 2:268 (1991).
6. J. B. Mehl and M. R. Moldover, *J. Chem. Phys.* **74**:4062 (1981).
7. M. R. Moldover, J. P. M. Trusler, T. J. Edwards, J. B. Mehl, and R. S. Devis, *J. Res. Natl. Bur. Stand. (U.S.)* **93**:85 (1988).
8. M. B. Ewing, M. L. McGrashan, and J. P. M. Trusler, *Metrologia* **22**:93 (1986).
9. A. R. H. Goodwin and M. R. Moldover, *J. Chem. Phys.* **93**:2741 (1990).
10. R. C. Reid, J. M. Prausnitz, and B. E. Poling, *The Properties of Gases & Liquids*, 4th ed. (McGraw–Hill, New York, 1987), p. 493.
11. C.-C. Piao, H. Sato, and K. Watanabe, *Proc. 3rd ASME/JSME Therm. Eng. Joint Conf.* **3**:435 (1991).
12. Z.-Y. Qian, Ph.D. dissertation (Department of Mechanical Engineering, Keio University, Yokohama, Japan, 1993).
13. M. O. McLinden, *Int. J. Refrig.* **13**:149 (1990).
14. M. Takahashi, C. Yokoyama, and S. Takahashi, *J. Chem. Eng. Data* **32**:98 (1987).